The Intensity Distribution of Faint Gamma-Ray Bursts Detected with BATSE

Jefferson M. Kommers,[1] Walter H. G. Lewin,[1] Chryssa Kouveliotou,[2,3] Jan van Paradijs,[4,5]
Geoffrey N. Pendleton,[4] Charles A. Meegan,[3] and Gerald J. Fishman[3]

ABSTRACT

We have recently completed a search of 6 years of archival BATSE data for gamma-ray bursts (GRBs) that were too faint to activate the real-time burst detection system running onboard the spacecraft. These "non-triggered" bursts can be combined with the "triggered" bursts detected onboard to produce a GRB intensity distribution that reaches peak fluxes a factor of ~ 2 lower than could be studied previously. The value of the $\langle V/V_{max} \rangle$ statistic (in Euclidean space) for the bursts we detect is 0.177 ± 0.006. This surprisingly low value is obtained because we detected very few bursts on the 4.096 s and 8.192 s time scales (where most bursts have their highest signal-to-noise ratio) that were not already detected on the 1.024 s time scale. If allowance is made for a power-law distribution of intrinsic peak luminosities, the extended peak flux distribution is consistent with models in which the redshift distribution of the gamma-ray burst rate approximately traces the star formation history of the Universe. We argue that this class of models is preferred over those in which the burst rate is independent of redshift. We use the peak flux distribution to derive a limit of 10% (99% confidence) on the fraction of the total burst rate that could be contributed by a spatially homogeneous (in Euclidean space) subpopulation of burst sources, such as type Ib/c supernovae. These results lend support to the conclusions of previous studies predicting that relatively few faint "classical" GRBs will be found below the BATSE onboard detection threshold.

Subject headings: gamma-rays: bursts

[1]Department of Physics and Center for Space Research, Massachusetts Institute of Technology, Cambridge, MA 02139; kommers@space.mit.edu

[2]Universities Space Research Association, Huntsville, AL 35800

[3]NASA/Marshall Space Flight Center, Huntsville, AL 35812

[4]University of Alabama in Huntsville, Huntsville, AL 35812

[5]University of Amsterdam, Amsterdam, Netherlands

1. Introduction

The origin of some, and possibly all, gamma-ray bursts (GRBs) at cosmological distances has been firmly established with the identification of X-ray, optical, and radio afterglows (Costa et al. 1997; Van Paradijs et al. 1997; Frail et al. 1997) and the subsequent measurement of cosmological redshifts for at least four of the optical afterglows and/or their host galaxies (Metzger et al. 1997; Kulkarni et al. 1998a; Djorgovski et al. 1999; Djorgovski et al. 1998). The objects responsible for producing the majority of GRBs, the gamma-ray bursters themselves, have yet to be understood, however. To obtain an understanding of the spatial distribution of sources and the distribution of their burst luminosities is a crucial step towards identifying the physical processes that produce GRBs.

Before the rapid follow-up of GRB afterglows was made possible by the *BeppoSAX* satellite, the only way to test hypotheses about the spatial and luminosity distributions was to fit parametric models to the measured characteristics of the bursts themselves. For this purpose the distribution of GRB intensities was used (see, for example, Fenimore et al. 1993; Rutledge, Hui, & Lewin 1995; Fenimore & Bloom 1995; Cohen & Piran 1995; Hakkila et al. 1996; and references therein). The effects of cosmological time dilation on the time profiles of bright versus faint bursts were also studied (Norris et al. 1995). Since optical spectroscopic redshifts are so far associated with only four (possibly five) bursts[1], number counts as a function of intensity remain an important tool for exploring the possible spatial and luminosity distributions of GRBs.

Several recent papers (Totani 1997, 1998; Wijers et al. 1998; Krumholz, Thorsett, & Harrison 1998; Mao & Mo, 1998) have used the observed GRB intensity distributions to investigate the possibility that the redshift distribution of gamma-ray bursters traces the global star formation history of the Universe. The motivation for this hypothesis is a collection of theoretical models in which GRBs are produced by stellar objects that evolve from their formation to their bursting phase on a time scale of $\sim$ 100 Myr or less. This group of models includes the merging of a neutron star with another neutron star or a black hole, the collapse of a massive star, and the collapse of a Chandrasekhar-mass white dwarf (see Wijers et al. 1998 for references). In these scenarios, the cosmological redshift distribution of the GRB rate should approximately follow the redshift distribution of the formation rate of stellar objects; in other words, the GRB rate should trace the global star formation history of the Universe. This hypothesis appears to solve some puzzling aspects of the observations, such as the "no host" problem (Schaefer et al. 1997; Wijers et al. 1998).

The star formation rate (SFR) as a function of redshift has been studied by Lilly et al. (1996), Fall, Charlot, & Pei (1996), Madau, Pozzetti, & Dickinson (1998), and Hughes et al. (1998). The principal result of these studies is that the SFR was substantially higher in the past. Between the present and $z \approx 1$ the SFR increases by a factor of ~ 10; it peaks somewhere in the range $z \approx 1$ to $z \approx 3$; and it decreases to a rate comparable to the present by $z \approx$ 4–5 (this last point remains uncertain).

Totani (1997), Wijers et al. (1998), Krumholz et al. (1998), and Mao & Mo (1998) all find that the GRB peak flux number counts can accommodate the hypothesis that the GRB rate follows the SFR. Among the important conclusions that these authors derive from this interpretation of the data are the following: 1) that the faintest gamma-ray bursts observed with the Burst and Transient Source Experiment (BATSE) onboard the *Compton Gamma Ray Observatory* (*CGRO*) are already produced at redshifts of $z \approx 3$ to $z \approx 6$ (Wijers et al. 1998; but see Section 4); and 2) that more sensitive experiments are unlikely to discover large numbers of faint GRBs (of the "classical" kind that are detected with current instruments) below the BATSE onboard detection threshold. The latter conclusion has important implications for the design and operation of future GRB detectors, which will test the behavior of GRB number counts at intensities well below the BATSE threshold.

We have recently completed a search of 6 years of archival data from BATSE for GRBs and other transients that did *not* activate the real-time burst detection system (or "trigger") running onboard the spacecraft. A GRB or other transient may fail to activate the BATSE onboard burst trigger for any of several reasons. The burst may be too faint to exceed the onboard detection threshold, it may occur while the onboard trigger is disabled for technical reasons,

[1] The proposed association of GRB 980425 with SN 1998bw (z = 0.008; Galama et al. 1998) may indicate a separate class of GRBs (Bloom et al. 1998). We will therefore consider that event separately (see section 3.2).

it may occur while the onboard trigger is optimized for detecting non-GRB phenomena, or it may artificially raise the onboard background estimate and be mistaken for a below-threshold event. Our search of the archival data is sensitive to GRBs with peak fluxes (measured over 1.024 s in the 50–300 keV energy range) that are a factor of ~ 2 lower than can be detected with the onboard trigger in its nominal configuration. Thus our search constitutes an experiment that is ~ 2 times more sensitive than those reported in the BATSE catalogs (Fishman et al. 1994; Meegan et al. 1996; Paciesas et al. 1999; Meegan et al. 1998).

In this paper we present results regarding the peak flux distribution of the GRBs detected with our "off-line" search of archival data. In section 2 we summarize some important aspects of our off-line search and we discuss the $\langle V/V_{max}\rangle$ statistic for the bursts we detected. We show that surprisingly few bursts are found on the 4.096 s and 8.192 s time scales that were not already detected on the 1.024 s time scale. In section 3 we fit parametric cosmological models to the observed differential peak flux distribution to compare scenarios in which the GRB rate follows the SFR with the model in which the co-moving GRB rate is independent of redshift. We also examine the possibility that a homogeneous (in Euclidean space) population of bursting objects could be contributing to the observed sample of GRBs. In section 4 we show how our results provide two independent arguments that favor models in which the GRB rate follows the SFR over models in which the GRB rate is independent of redshift.

2. The Search for Non-Triggered GRBs

The details of our off-line search of the BATSE data are discussed in Kommers et al. (1997). We have merely extended the search from covering 345 days of the mission to covering 2200 days. We have also made minor modifications to our peak flux estimation procedure in order to secure better relative calibration between our peak fluxes and those in the 4B catalog (Paciesas et al. 1999). The extended catalog of non-triggered events will be provided and discussed in the Non-Triggered Supplement to the BATSE Gamma-Ray Burst Catalogs (Kommers et al. 1999b). Here we address only those aspects of the search that are relevant to the GRB intensity distribution analysis.

We use the data from the Large Area Detectors that provide count rates in 4 energy channels with 1.024 s time resolution (the data type designated "DISCLA" in the flight software; Fishman et al. 1989). These data are searched for statistically significant count rate increases to identify candidate burst events. The many candidate events ("off-line triggers") are then visually inspected to separate astronomically interesting transients from instrumental and terrestrial effects. To be considered a GRB, a candidate must exhibit significant signal in the 50–300 keV range (DISCLA channels 2 and 3) and it must *lack* any characteristics that would associate it with a solar flare, Earth magnetospheric particle precipitation, or other non-GRB origin. Since the DISCLA data are (nearly) continuously recorded, our search detects some bursts that already activated the onboard burst trigger; we call these events "onboard-triggered bursts." Bursts that were detected *exclusively* by our search of archival data are called "non-triggered bursts."

In addition to searching at the 1.024 s time resolution of the DISCLA files, we also search the data binned at 4.096 s and 8.192 s time resolution. The longer time bins provide greater sensitivity to faint bursts that have durations longer than ~ 4 s or ~ 8 s. The specific time profile of each burst determines which of these three time scales is the most sensitive. For this reason the searches on each time scale should be considered separate experiments.

Our search covers 1.33×10^8 s of archival data spanning the time from 1991 December 9 to 1997 December 16. In these data we detected 2265 GRBs, of which 1392 activated the onboard burst trigger and 873 did not. We will refer to these 2265 GRBs as the "off-line GRB sample." During the same time period, the onboard burst trigger detected 1815 GRBs. The $1815 - 1392 = 423$ bursts that were detected by the onboard burst trigger but that were *not* detected by our search either occurred during gaps in the archival DISCLA data or had durations much less than the 1.024 s time resolution (so they did not achieve adequate statistical significance in the archival data).

Note that because the best time resolution available to our retrospective search is 1.024 s, all results in this paper pertain to bursts with durations longer than about 1 s. Thus, the population of "short" (duration less than ~ 2 s) bursts that contributes to the bimodal GRB duration distribution (Kouveliotou et al. 1993) is not well represented in the off-line sample. An estimate for the fraction of bursts that our search is likely to miss because of our time resolution can be obtained from the 4B catalog. Although 21% of GRBs for which both durations and fluences were available had $T_{90} < 1.024$ s, only 7% had both $T_{90} < 1.024$ s and fluences too small to create adequate statistical significance in the 1.024 s data (Paciesas et al. 1999).

For each of the 873 non-triggered GRBs we have estimated a peak flux in the 50–300 keV range based on the time bin with the most counts above background. For 1288 of the 1392 onboard-triggered GRBs, we used the peak fluxes from the current BATSE GRB catalog (Meegan et al. 1998). For the remaining 104 onboard-triggered bursts, peak fluxes were not available from the current burst catalog; we estimated peak fluxes for them using our own techniques as we did for the non-triggered bursts.

Since the onboard trigger criteria were changed for a variety of reasons during the time spanned by our search, we adopt for the nominal onboard detection threshold the value 0.3 ph cm^{-2} s^{-1} in the 50–300 keV range. At this peak flux the onboard trigger efficiency is ≈ 0.5 (Paciesas et al. 1999). With this estimate, 551 of our 873 non-triggered bursts were below the nominal onboard detection threshold. The rest were not detected onboard for the reasons cited previously.

2.1. Trigger Efficiency

To determine the peak flux threshold of the off-line GRB sample, the trigger efficiency $E_1(P)$ of our off-line search has been calculated using the techniques described in Kommers et al. (1997). This quantity is the probability that a burst that occupies exactly one 1.024 s time bin with a peak flux P will be detected by the off-line search algorithm. $E_1(P)$ is well represented (within the uncertainties of the calculation owing to variations in the background rates) by the following function:

$$E_1(P) = \frac{1}{2}\left[1 + \mathrm{erf}(-3.125 + 16.677P)\right], \qquad (1)$$

where erf(x) is the standard error function and P is given in units of photons cm^{-2} s^{-1} in the 50-300 keV band. This equation is plotted as the dashed line in Figure 1. Error bars on the grid points of the calculation (diamonds) represent the sample standard deviation of the calculated probabilities owing to variations in the background rates. For comparison, the BATSE trigger efficiency from the 4B catalog (Paciesas et al. 1999) is plotted as the dotted line (grid points are indicated by open squares). Equation 1 tends to *underestimate* the probability that a typical GRB will be detected, however. This is because many GRBs in our sample last longer than 1.024 s; therefore, these bursts have more than one statistical chance to be included in the sample.

Suppose the peak of a burst occupies N time bins, so that the burst has effectively N statistical chances to be detected. Then the probability that the burst is detected can be approximated as unity minus the probability that the burst *fails* to be detected in all N trials:

$$E_N(P) = 1 - \left[1 - E_1(P)\right]^N . \qquad (2)$$

Since the number of chances N is not known for GRBs *a priori*, the actual probability of detection $E(P)$ is obtained by marginalizing $E_N(P)$ over the distribution of N for bursts with peak fluxes near P:

$$E(P) = \frac{\sum h(N,P)\, E_N(P)}{\sum h(N,P)}. \qquad (3)$$

Our estimate for $h(N,P)$, the histogram of the various integer values of N for bursts with peak fluxes near P, was obtained from the detected sample of bursts by counting, for each burst, the number of time bins with count rates that were within one standard deviation of the peak count rate. For purposes of illustration, Figure 2 shows the histogram of N for bursts with peak fluxes in the range 0.1–0.4 ph cm^{-2} s^{-1}. The resulting function $E(P)$ is well represented (to within the uncertainties of the calculation) by the formula

$$E(P) = \frac{1}{2}\left[1 + \mathrm{erf}(-4.801 + 29.868P)\right]. \qquad (4)$$

This equation expresses our best estimate of the trigger efficiency of our off-line search on the 1.024 s time scale. It is plotted as the solid line in Figure 1. The efficiency of our search falls below 0.5 at a peak flux of 0.16 ph cm^{-2} s^{-1}.

If we had not made some correction for the effect of time profiles on the single-time-bin burst detection probabilities, we would have substantially underestimated our trigger efficiency near the detection threshold ($\sim$ 0.2 ph cm^{-2} s^{-1}). We note that this type of correction to the single-time-bin trigger efficiency should also be applied when using the trigger efficiencies given in the 1B, 2B, 3B, and 4B catalogs (Fishman et al. 1994; Meegan et al. 1996; Paciesas et al. 1999). Similar considerations are addressed by in't Zand & Fenimore (1994) and Loredo & Wasserman (1995).

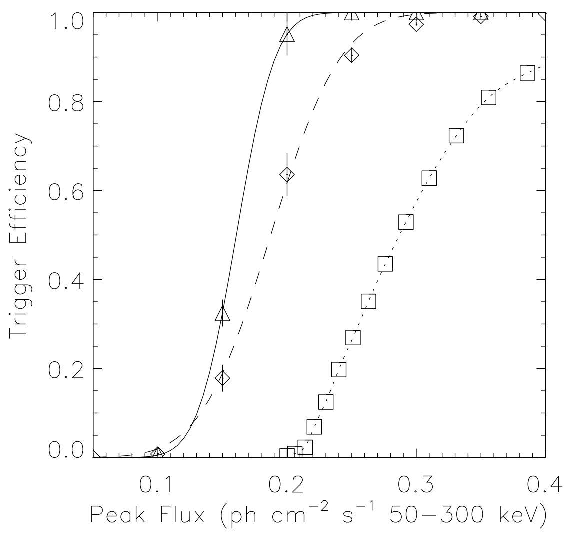

Fig. 1.— Trigger efficiency for our off-line search. The grid points of the calculations are plotted as individual symbols. Error bars represent the standard deviations of the calculated probabilities owing to variations in the background rates. The dashed line (equation 1) shows the probability that a burst occupying a single time bin is detected by our search. The solid line (equation 4) shows the marginal probability that a burst is detected by our search, given that some bursts longer than 1.024 s have more than one statistical chance to be detected. For comparison, the dotted line shows the trigger efficiency from the 4B catalog; no uncertainties are available for the grid points (squares).

2.2. $(C_{min}/C_{max})^{3/2}$ Distribution

As successively more sensitive instruments have been used to produce GRB catalogs, it has been customary to give the value of the $\langle V/V_{max}\rangle$ statistic for the detected bursts (Schmidt, Higdon, & Hueter 1988). For photon counting experiments like BATSE, it is not strictly $\langle V/V_{max}\rangle$ that is typically calculated, but rather $\langle (C_{min}/C_{max})^{3/2}\rangle$, where C_{min} is the threshold count rate and C_{max} is the maximum count rate measured during the burst. The departure of $\langle (C_{min}/C_{max})^{3/2}\rangle$ from the value of $\frac{1}{2}$ expected for a population of bursters distributed homogeneously in Euclidean space (with a well-behaved, but otherwise arbitrary luminosity distribution) has been firmly established (Meegan et al. 1992; Meegan et al. 1996). Since the discovery that most GRBs originate at cosmological distances, the quantity $\langle (C_{min}/C_{max})^{3/2}\rangle$ can no longer be interpreted as $\langle V/V_{max}\rangle$. Nevertheless, it is useful to compare the values of $\langle (C_{min}/C_{max})^{3/2}\rangle$ obtained by successively more sensitive experiments, including the value obtained for the bursts detected with our search.

Table 1 lists various missions and the values they obtained for $\langle (C_{min}/C_{max})^{3/2}\rangle$. The trend towards lower values of $\langle (C_{min}/C_{max})^{3/2}\rangle$ with more sensitive experiments indicates that increasing the accessible survey volume by decreasing the flux threshold does not lead to the detection of large numbers of faint bursts.

The value of $\langle (C_{min}/C_{max})^{3/2}\rangle$ for the 2265 GRBs detected by our search[2] is 0.177 ± 0.006. *This is the lowest value ever obtained for a sample of GRBs.* The cumulative distribution of $(C_{min}/C_{max})^{3/2}$ for our GRBs is shown in Figure 3. The flattening of this curve in the range $0.5 < (C_{min}/C_{max})^{3/2} < 1.0$ shows that over 90% of the GRBs we detect are above threshold (on at least one of the 3 time scales) by a factor of at least $(0.5)^{-3/2} = 1.6$.

The reason for this low value of $\langle (C_{min}/C_{max})^{3/2}\rangle$ is the fact that most of the bursts we detected had their maximum signal-to-noise ratios on the 4.096 s and 8.192 s time scales, yet surprisingly few bursts were detected *only* on these longer time scales. For each burst we compute the values of $(C_{min}/C_{max})^{3/2}$ on each of the 3 time scales. The largest of the three values for each burst is used in taking the average. In

[2]This value supersedes the ones given in Kommers et al. (1996, 1997, 1998), which are incorrect due to a programming error. An erratum has been submitted (Kommers et al. 1999a).

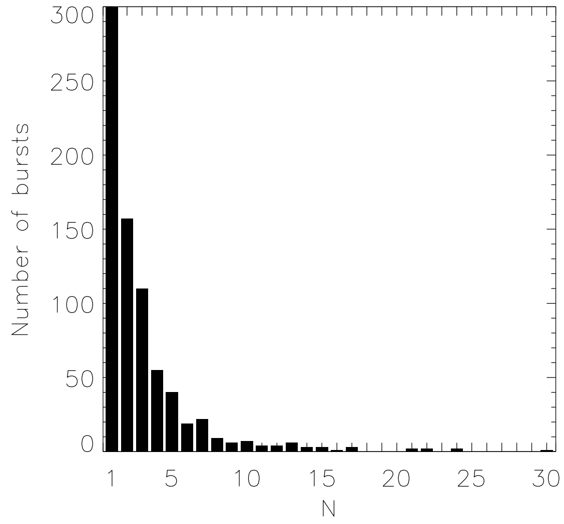

Fig. 2.— Histogram of N, the number of time bins within one standard deviation of the peak count rate, for bursts with peak fluxes in the range 0.1–0.4 ph cm^{-2} s^{-1}.

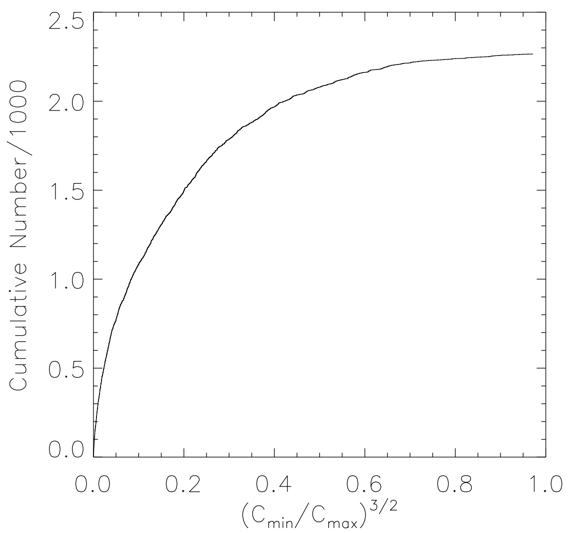

Fig. 3.— Cumulative distribution of $(C_{min}/C_{max})^{3/2}$ for the off-line GRB sample. The dramatic flattening of the curve above $(C_{min}/C_{max})^{3/2} = 0.5$ shows that few of the GRBs detected in our search are just barely above the detection threshold on all 3 time scales (1.024 s, 4.096 s, and 8.192 s).

Euclidean space this corresponds to taking for each burst the *smallest* value of $\langle V/V_{max}\rangle$. Since 72.0% of the bursts we detected have T_{90} durations (Koshut et al. 1996) longer than 8 s, we expect the average $\langle (C_{min}/C_{max})^{3/2}\rangle$ to be dominated by values measured on the 8.192 s time scale.

In fact, the average $\langle (C_{min}/C_{max})^{3/2}\rangle = 0.177 \pm 0.006$ includes 520 values measured on the 1.024 s time scale, 491 values measured on the 4.096 s time scale, and 1254 values measured on the 8.192 s time scale. Yet only 105 bursts were detected *exclusively* on either of the 4.096 or 8.192 s time scales (or both). Many of the bursts that are barely above the detection threshold on the 1.024 s time scale are well above the detection threshold on the longer time scales. Thus very few bursts are found to be just barely above our detection threshold on all 3 time scales, and this accounts for the low value of $\langle (C_{min}/C_{max})^{3/2}\rangle$. Restricting our calculation to use *only* count rates measured on the 1.024 s time scale (and bursts detected on the 1.024 s time scale) gives a larger value, $\langle (C_{min}/C_{max})^{3/2}\rangle = 0.247 \pm 0.006$.

Roughly, the 4.096 s search should be $\sim$ 2 times more sensitive than the 1.024 s search for bursts that maintain their peak flux for at least $\sim$ 4 s, and the 8.192 s search should be yet more sensitive. Therefore our lack of GRB detections exclusively on the longer time scales indicates either 1) a substantial paucity of faint, long bursts below the threshold of our 1.024 s search, or 2) that during our visual inspection of the off-line triggers we have tended to classify a substantial number of faint, long GRBs as other (non-GRB) phenomena. We feel that both alternatives must be present at some level.

A review of the non-GRB off-line triggers suggests that events resembling faint, long GRBs that illuminate the same detectors as a known, bright, variable X-ray source are more likely to be attributed to variability from the X-ray source than to be classified as GRBs. There is also a tendency to classify bursts that have directions consistent with the Sun as solar flares. A secondary evaluation of the event classifications suggests that between 50 and 200 (this range represents the central 90% confidence interval), with a most likely value of 86, GRBs have been misclassified in this way. The corresponding "loss rate" is between 2% and 8% (most likely 4%) of the total 2265 bursts in the off-line sample. This is not enough to fully explain, as experimental error, the dearth of faint, long bursts below our 1.024 s threshold.

2.3. Peak Fluxes

Detailed comparisons of cosmological models with the data require intensity distributions in physical units. We have chosen to do the analysis in terms of the burst rate as a function of peak photon flux measured over 1.024 s in the energy range 50–300 keV. Compared with the fluence (total energy per unit area deposited in the detector by the burst) we prefer peak photon flux for the purposes of intensity analysis. The peak photon flux can be obtained more reliably from the raw count data and it is more directly related to our ability to detect bursts.

Of the 2265 GRBs detected by our search, we chose to include in our peak flux analysis only those that were detected on the 1.024 s time scale, so that equation 4 gives the detection efficiency. We also chose to use only those bursts with peak fluxes in the range 0.18–20.0 ph cm^{-2} s^{-1}. The lower limit ensures that the off-line trigger efficiency exceeds 0.8 for the range of intensities used in the analysis, and the upper limit excludes very bright bursts which are too rare to provide adequate counting statistics in narrow peak flux bins. With these cuts on the data, we are left with 1998 peak flux measurements. To fit the differential intensity distribution, we bin the 1998 bursts into 25 peak flux intervals that were chosen to be approximately evenly spaced in the logarithm of P. The spacing is $\Delta \log P \approx 0.05$ in the range $0.18 < P < 1.0$, $\Delta \log P \approx 0.1$ in the range $1.0 < P < 7.9$, and there is a final broad bin for the range $7.9 < P < 20.0$. Uncertainties in the number of bursts ΔN_{obs} in each bin are taken to be $\pm\sqrt{\Delta N_{obs}}$. The burst rate is computed by dividing the number of bursts in each bin by the live time of the search (1.33×10^8 s $= 4.21$ yr) and the mean solid angle visible to the BATSE detectors ($0.67 \times 4\pi$). Table 2 gives the peak flux intervals, number of bursts, and burst rate for each bin.

3. Cosmological Model Comparison

Many investigators, in scores of papers, have shown the consistency of the GRB peak flux distribution with various cosmological models (see, for example, Wijers et al. 1998; Loredo & Wasserman 1998; Hakkila et al. 1996; Horack et al. 1996; Rutledge, Hui, & Lewin 1995; Fenimore & Bloom 1995; and references therein). As shown in the previous section, the off-line GRB sample extends the observed GRB intensity distribution to peak fluxes that are lower by a factor of ~ 2 than could be studied previously. While it is unlikely that a factor of ~ 2 will yield stringent new model constraints, it remains of interest to note a few cosmological models that provide good fits to the extended GRB peak flux distribution. These can be used to set limits on the rate of GRBs that may come from a nearby, spatially homogeneous subpopulation of burst sources.

3.1. Purely Cosmological Models

To limit the number of free parameters that must be considered, our choice of cosmological world model is the Einstein-de Sitter model ($\Omega = 1$, $\Lambda = 0$, $q_0 = \frac{1}{2}$; Weinberg 1972). This cosmology has been used by many other investigators so it allows easy comparison of results. Where needed, we assume a Hubble constant $H_0 = 70\ h_{70}$ km s^{-1} Mpc^{-1}. We also assume that bursters are distributed isotropically, so the only interesting parameter in the burster spatial (redshift) distribution is the radial coordinate $r(z)$ from Earth. The following derivation of the expected peak flux distributions follows the discussions in Fenimore & Bloom (1995) and Loredo & Wasserman (1997).

In general the rate of bursts R per unit interval in peak flux P observable at Earth is given by

$$\frac{dR}{dP} = \int dL \int dz\ \frac{\partial^2 R}{\partial L\, \partial z}\ \delta(P - \Phi(L,z)), \qquad (5)$$

where L is the equivalent isotropic peak luminosity of the burst at the source, z is the redshift parameter, $\partial^2 R/\partial L\, \partial z$ is the rate of bursts per unit L per unit redshift interval, $\delta(x)$ is the Dirac delta function, and $\Phi(L,z)$ is the peak photon flux measured at Earth for a burst with peak luminosity L located at redshift z. We will assume that the redshift and luminosity distributions are independent, so that the burst rate as a function of L and z is given by

$$\frac{\partial^2 R}{\partial L\, \partial z} = \frac{4\pi c R_0}{H_0}\ \psi(L)\rho(z)\ \frac{r^2(z)}{(1+z)^2\ \sqrt{1+z}} \qquad (6)$$

where R_0 is an overall normalization, $\psi(L)$ is the distribution of burst luminosities (normalized to unity), $\rho(z)$ is the distribution of the co-moving burst rate as a function of redshift (normalized to unity on the interval $0 < z < 10$), and $r(z) = (2c/H_0)(1 + z - \sqrt{1+z})/(1+z)$ is the co-moving radial coordinate.

The peak flux $\Phi(L,z)$ observed at Earth in the 50–300 keV energy range, where the BATSE burst trigger is sensitive, depends on the intrinsic spectrum of the

GRB. We write it as

$$\Phi(L,z) = \frac{L\ K(z)}{4\pi\ (1+z)\ r^2(z)}. \tag{7}$$

The spectral correction function $K(z)$ depends on the shape of the burst photon energy spectrum at the source. The observed GRBs have a variety of spectral shapes, and in the cosmological scenario these observed spectra have been redshifted according to the (unknown) redshifts of the sources.

To account for the spectral variety of GRBs we use the spectral fits of Band et al. (1993). To account for the unknown redshift factors for these spectra, we use the procedure described in Fenimore & Bloom (1995). The peak fluxes of the bursts for which Band et al. (1993) derived spectral fits are used in conjunction with the cosmological model under consideration to self-consistently estimate the redshift factors for the fitted spectra. We assume that the ith burst fitted by Band et al. (1993) has exactly the mean intrinsic peak luminosity in the cosmological model being considered: $L_i = \int dL'\ L'\psi(L')$, where the shape of $\psi(L)$ depends on the parameters of the model luminosity function. We then solve for the redshift z_i which the fitted burst i must have had to produce the peak flux listed for it in the current BATSE GRB catalog (Meegan et al. 1998). Fifty-one of the bursts fitted by Band et al. (1993) had peak fluxes available. For each of their spectral shapes $\phi_i(E)$ the spectral correction function takes the form

$$K_i(z) = \frac{\int_{50(1+z)/(1+z_i)}^{300(1+z)/(1+z_i)} dE\ \phi_i(E)}{(1+z_i)\ \int_{30/(1+z_i)}^{2000/(1+z_i)} dE\ E\phi_i(E)}. \tag{8}$$

The integrals in the denominator and numerator convert the model parameter L, which represents the peak luminosity in the 30–2000 keV range at the source, to the observed photons cm^{-2} s^{-1} in the 50-300 keV band at Earth. The burst rate expected in the BATSE band pass for the ith spectral shape $\phi_i(E)$ is then (from equation 5)

$$\left(\frac{dR}{dP}\right)_i = \frac{16\pi^2 c R_0}{H_0} \times \int dz\ \frac{\rho(z)\ r^4(z)}{(1+z)\ \sqrt{1+z}\ K_i(z)}\ \psi\left(\frac{4\pi\ (1+z)\ r^2(z)\ P}{K_i(z)}\right). \tag{9}$$

The limits on the integral are determined by the range of z for which $\psi(4\pi(1+z)r^2(z)P/K_i(z))$ is non-zero at the given P.

To estimate the observed distribution of bursts, which includes a variety of spectral shapes, we average Equation 9 over the 51 spectral correction functions $K_i(z)$. This procedure is equivalent to marginalizing the unknown spectral parameters of the observed bursts (i.e., those in the off-line sample) to obtain the posterior rate distribution. The 51 spectra from Band et al. (1993) are furnishing estimates of the prior distributions of the spectral parameters. The expectation value of the observed burst rate for peak fluxes between P_1 and P_2 is then

$$\Delta R(P_1, P_2) = \int_{P_1}^{P_2} dP\ E(P)\ \left\langle \frac{dR}{dP} \right\rangle, \tag{10}$$

where $\langle dR/dP \rangle$ is the mean rate estimated from the 51 observed spectra and $E(P)$ is the detection efficiency.

The use of the Band et al. spectra increases the computational cost of the rate model by a factor of $\sim$ 50 over using a single "universal" burst spectrum. We found that a simple power-law form for the GRB photon energy spectrum—as has been used by many previous studies—predicts significantly different burst rates at low peak fluxes than does equation 10. Since we are interested in the behavior of the burst rate at low peak fluxes, we felt that the analysis based on the full 51 Band et al. spectra would be more reliable. Similar conclusions are reached by Fenimore & Bloom (1995) and Mallozzi, Pendleton, & Paciesas (1996).

For comparison with the results of previous studies, we chose two forms for the luminosity distribution. The first is a monoluminous (standard candle) distribution. The second is a truncated power-law,

$$\psi(L) = \begin{cases} \frac{1}{L \log(L_{max}/L_{min})} & \beta = 1 \\ \frac{(1-\beta)\ L^{-\beta}}{L_{min}^{1-\beta} - L_{max}^{1-\beta}} & \beta \neq 1 \end{cases} \tag{11}$$

with $\psi(L) = 0$ if $L < L_{min}$ or $L > L_{max}$. The normalization factors ensure that $\int dL\ \psi(L) = 1$.

The standard candle distribution, though useful for comparison with other results, is ruled out by the observed peak fluxes of the four bursts for which associated optical redshifts have been measured. For GRBs 970508, 971214, 980613, and 980703 the inferred equivalent isotropic peak luminosities in the 30–2000 keV energy range are given in Table 3. To calculate each of these peak luminosities, we have used the observed 50–300 keV peak flux (on the 1.024 s time scale) in combination with the observed redshift to find the expectation value of the intrinsic luminosity averaged over the 51 Band et al. spectra.

This procedure is the one used in our modeling, so it was used on these four bursts also, to facilitate comparisons with the models (see section 4). The peak luminosities estimated here are somewhat higher by factors of ~ 3 to ~ 6 than those reported elsewhere (e.g., Krumholz et al. 1998). This is because the spectral shapes fitted by Band et al. (1993) generally become steeper at high energies, so a source at high redshift must be more luminous to produce the flux observed at Earth than it would have to be if the spectrum did not fall off so rapidly at higher energies. These differences illustrate the importance of using the most realistic spectral models available rather than simple power-laws when analyzing the GRB intensity distribution.

A variety of spatial, or rather redshift, distributions for the bursters have been used in previous studies of the GRB intensity distribution. With up to 4 free parameters already incorporated into our burst rate models (the overall normalization R_0, and the parameters of the power-law luminosity function β, L_{min}, and L_{max}) there is little hope of constraining any additional free parameters in the redshift distribution. Here we explore 3 specific models of the redshift distribution that contain no free parameters. The two physical scenarios we examine are 1) that the co-moving burst rate is independent of redshift between $z = 0$ and $z = 10$, and 2) that the co-moving GRB rate is proportional to the star formation rate (SFR).

For the GRB rate model that is independent of redshift, $\rho(z) = 0.1$ for $0 < z \leq 10$ and $\rho(z) = 0$ for $z > 10$. We refer to this redshift distribution as "model D1."

For the case where the burst rate follows the star formation history of the Universe, we use two slightly different parameterizations of the SFR. The first is the SFR deduced from the rest-frame ultraviolet luminosity density, with the functional form given in footnote 1 of Madau, Della Valle, & Panagia (1998). In this estimation the SFR peaks around z =1–1.5. A SFR of roughly this form has been used by several previous studies of the GRB intensity distribution (Totani 1997; Wijers et al. 1998; Krumholz et al. 1998). We refer to this redshift distribution as "model D2."

The second SFR parameterization assumes that the SFR—and thus the GRB rate—tracks the total output of radio-loud AGN. In this scenario the SFR peaks at z =2–3 (Hughes et al. 1998; Dunlop 1998). This form of the SFR appears to be more consistent with recent results from SCUBA (Hughes et al. 1998) which are not susceptible to the same problems of dust obscuration as the determination by Madau et al. (1998). The specific functional form we use is a best-fit analytic model to points measured by hand from Figure 6 of Hughes et al. (1998): $\rho(z) \propto 0.00360 + 0.0108 \exp(2.76z - 0.573z^2)$. This approximation appears to be accurate to within 5% for the redshift range $1 < z < 4$. (At lower and higher redshifts the formula likely underestimates the actual rate of star formation; but this is no great concern as it is the redshift of the peak SFR that is of primary interest.) We refer to this redshift distribution as "model D3."

With choices for $\psi(L)$ and $\rho(z)$ as discussed, we fit equation 10 to the data in Table 2 by minimizing the χ^2 statistic. In all cases, we found that the parameter L_{max} was not well constrained: variations in L_{max} did not change the minimum χ^2 by a significant amount. The (mathematical) reason for this is that the integrand in equation 9 is a decreasing function of z for plausible values of β, so that varying the upper limit (z_{max} corresponding to L_{max} for the given P) causes only small changes in the value of the integral. Accordingly, all the results reported here set $L_{max} \equiv 1000 L_{min}$. The free parameters are thus R_0 and L_0 in the cases of the standard candle models, and R_0, β, and L_{min} in the cases of the power-law luminosity distribution models. The results of the fits are listed in Table 4 and Table 5. Uncertainties on the fitted parameters correspond to 68% confidence limits for 2 ($\Delta\chi^2 = 2.3$) or 3 ($\Delta\chi^2 = 3.5$) interesting parameters, respectively (Avni 1976).

Model D1 (constant burst rate density as a function of redshift) produces an acceptable fit for the standard candle luminosity distribution. The probability of getting $\chi^2 > 32.3$ for 23 degrees of freedom is 0.094. Adding one more free parameter (β) for the power-law luminosity distribution produces an insignificant change in the minimum χ^2. Furthermore, the high value of β in the best-fit power-law distribution indicates a very narrow range of peak luminosities.

Model D2 (burst rate density follows the SFR as determined by Madau et al. 1998) produces a formally unacceptable fit in the monoluminous case. But it achieves an excellent fit (χ^2 per degree of freedom = 0.81) for the power-law luminosity distribution. The F-test estimates a probability of 1.5×10^{-7} that the improvement in χ^2 is due to chance, justifying the inclusion of the additional parameter in the power-law luminosity function model. The value of β in this model is remarkably well-constrained. If the other fit parameters are regarded as "uninteresting" then the 90% ($\Delta\chi^2 = 2.7$) and 99% ($\Delta\chi^2 = 6.6$) confidence intervals (Avni 1976) on β are 2.0–2.3 and 1.8–2.6, respectively.

Model D3 (burst rate density follows the output of radio-loud AGN) produces formally acceptable fits with both the standard candle and power-law luminosity distributions. The power-law luminosity distribution achieves a significantly lower χ^2, however. The F-test estimate of the probability that the improvement is due to chance is 1.5×10^{-3}.

Figure 4 plots the differential peak flux distributions for the best-fit models with power-law luminosity distributions. For all three best-fit models the value of $\langle (P_{min}/P)^{3/2} \rangle$ is consistent with the value of $\langle (C_{min}/C_{max})^{3/2} \rangle$ measured for the sample (see section 2.2). Extrapolating the best-fit models to peak fluxes lower than those included in our data shows very different behaviors. Model D1 (dot-dashed lines) predicts a dramatically higher burst rate at low peak fluxes than do models D2 (solid line) and D3 (dashed line).

In each model the best-fit parameters for the power-law luminosity function yield our best estimate of the parameters of the *intrinsic* distribution of GRB peak luminosities. The distribution of peak luminosities of the *observed* bursts is different, however, because the most luminous bursts are sampled from a much larger volume than than are the least luminous bursts. Even though high luminosity bursts are infrequent, the geometrical advantage of sampling them from a larger volume means that they will be over-represented in a sample of bursts observed over a fixed time interval. The distribution of peak luminosities for the observed bursts is the "effective luminosity function" (see Loredo & Wasserman 1997 for further discussion). For the best-fit parameters of model D1 the effective luminosity function is a power-law that is less steep than that of the intrinsic luminosity function. We find $\beta_{\rm eff}^{\rm D1} = 2.8$ for the effective luminosity function versus $\beta = 4.6$ for the intrinsic one. The power-law slopes of the effective luminosity functions for models D2 and D3 are $\beta_{\rm eff}^{\rm D2} = 1.6$ and $\beta_{\rm eff}^{\rm D3} = 1.9$, respectively.

Similarly, the distribution of the GRB rate as a function of redshift for the observed bursts is not identical to the intrinsic redshift distribution given by $\rho(z)$

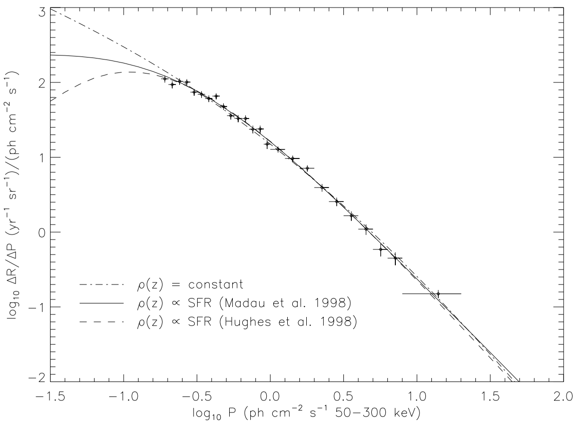

Fig. 4.— Best-fit cosmological models with power-law luminosity distributions. Units of R are bursts $\rm yr^{-1}\ sr^{-1}$, and those of P are $\rm ph\ cm^{-2}\ s^{-1}$ in 50–300 keV. The dot-dashed line corresponds to model D1 (co-moving burst rate is independent of redshift). The solid line shows model D2 (burst rate follows the rest-frame ultraviolet luminosity density) and the dashed line shows model D3 (burst rate follows the output of radio-loud AGN). Measured rates are shown with 1σ vertical error bars; horizontal error bars indicate the bin widths. The best-fit model curves displayed here have not been corrected for detection efficiency.

(see Loredo & Wasserman 1997). Figure 5 shows the effective redshift distributions for the best-fit models D1, D2, and D3. In all 3 models the effective redshift distribution cuts off at a lower redshift than does the corresponding intrinsic redshift distribution. The mean redshifts of the observed bursts in the best-fit models D1, D2, and D3 are $\langle z \rangle^{D1} = 0.86$, $\langle z \rangle^{D2} = 1.4$, and $\langle z \rangle^{D3} = 1.9$, respectively. The maximum redshifts of the bursts in models D1, D2, and D3 are not precisely determined, but the observed redshift distributions cut off around $z^{\rm D1}_{\rm max} \approx 1.5$, $z^{\rm D2}_{\rm max} \approx 2$, and $z^{\rm D3}_{\rm max} \approx 3$, respectively (see Figure 5).

It is interesting to compare the rate of bursts that are seen with the off-line search to the total rate of bursts that occur in the Universe, subject to the cosmological rate models we are considering. The fraction of bursts that are detected with BATSE is given by the integral of the effective redshift distribution for the off-line search (over the range $0 < z < 10$) divided by the integral of the effective redshift distribution that would be visible to a "perfect detector" which can detect infinitely faint bursts, multiplied by the live-time (0.70) and sky exposure (0.67) fractions. In the best-fit models D1, D2, and D3, it follows that the off-line search detects $\sim 14\%$, $\sim 30\%$, and $\sim 37\%$, respectively, of the bursts that occur in the Universe. Of course, these estimates can apply only to bursts with energy spectra and durations of the kind that are accessible to the off-line search. If BATSE had 100% live-time and no Earth blockage, then in model D1 30% of the bursts that occur could be detected with the off-line search. In models D2 and D3, 65% and 78%, respectively, of the bursts that occur could be detected with the off-line search.

It is customary to quote the rate of GRBs as the co-moving rate per unit volume at $z = 0$, a quantity often denoted by ρ_0 with units of Gpc^{-3} yr^{-1} (Fenimore & Bloom 1995, Wijers et al. 1998). The model parameter R_0 is related to ρ_0 by $\rho_0 = 4\pi R_0 \rho(0)$. Table 6 lists the values of ρ_0 corresponding to the best-fit values of R_0 for the standard-candle GRB models. Table 7 does the same for the GRB models with a power-law luminosity function. This burst rate can be converted into an event rate per "typical" galaxy using the space density of such galaxies. Here, a "typical" galaxy is taken to be one with a luminosity L^* equal to the characteristic luminosity of galaxies in the Schechter function (Schechter 1976). Loveday et al. (1992) report the mean space density of L^* galaxies to be $(4.8 \pm 0.6)\ 10^{-3}\ h^3_{70}$ Mpc^{-3}. With this

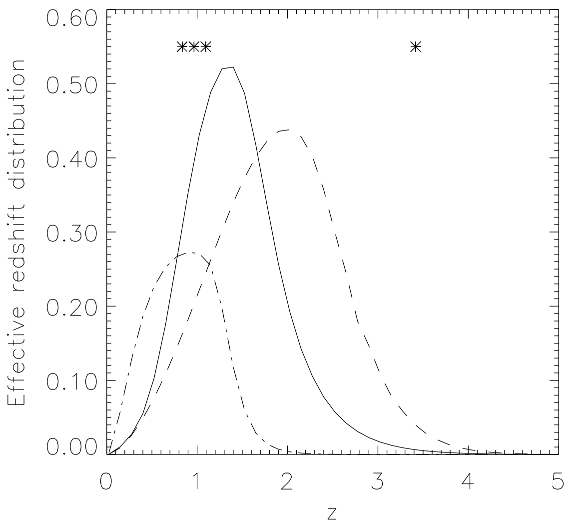

Fig. 5.— Redshift distribution of the burst rate for observed bursts (i.e., the effective differential burst rate as function of redshift). The distributions are normalized so that the integral of the distribution visible to a "perfect" detector with no sensitivity limit is unity. The dot-dashed line corresponds to a constant burst rate as a function of redshift (model D1). The solid line corresponds to the model (D2) where the burst rate traces the SFR as determined by Madau et al. (1998). The dashed line corresponds to the model (D3) where the burst rate traces the output of radio-loud AGN (Hughes et al. 1998). In model D1 the off-line search detects a smaller percentage of the bursts that occur than it does in models D2 and D3. The redshifts associated with GRBs 970508, 971214, 980613, and 980703 are marked with asterisks.

conversion, the co-moving rate of GRBs at $z = 0$ can be expressed in GEM (Galactic Events per Million years), which is the rate of GRBs in an L^* galaxy. This quantity is also listed in Tables 6 and 7.

3.2. Limits on a Possible Homogeneous Subpopulation

The discovery of the unusual Type Ib/c supernova SN 1998bw in the X-ray error box of GRB 980425 has fueled speculation that the supernova (SN) produced the GRB (Galama et al. 1998; Iwamoto et al. 1998; Kulkarni et al. 1998b). It has been suggested that such events (the supernova-GRBs, or "S-GRBs") may constitute a subclass of all GRBs (Bloom et al. 1998). In this subsection we discuss what fraction of all GRBs could belong to such a subclass assuming that the remaining bursts come from the "reasonable" cosmological scenarios discussed previously.

If the inferred peak luminosity of GRB 980425 (assuming a distance corresponding to the redshift $z = 0.0085$ of SN 1998bw; Tinney et al. 1998) is typical of S-GRBs, then the bursts in this subclass are detectable within a volume of radius ~ 100 Mpc (Bloom et al. 1998). Within this volume, we assume the spatial distribution of Type Ib/c SNe to be approximately homogeneous. Thus the cumulative intensity distribution of S-GRBs can be expected to follow a $-3/2$ power-law. This conclusion follows for any well-behaved distribution of intrinsic luminosities as long the spatial distribution does not deviate from homogeneity within the volume sampled by our detectors. Since the observed intensity distribution of all GRBs deviates strongly from the $-3/2$ power-law, it can be used to set an upper limit on the fraction of all GRBs that can come from a subclass which obeys the $-3/2$ power-law. In this respect, the faint end of the peak flux distribution (as explored by our off-line search) provides the most stringent constraints.

A model-independent limit on the fraction of bursts that might come from a nearby homogeneous population can be obtained from the histogram of $(C_{min}/C_{max})^{3/2}$ for the observed bursts. Any homogeneous subpopulation is expected to contribute a constant number of bursts to each bin in the histogram. Thus the bin with the fewest number of bursts sets an upper limit on the total number of bursts that could come from the subpopulation. The bursts detected with our search have already been used to set an upper limit of 5–6% on the fraction of bursts that could come from a homogeneous subpopulation; this limit is therefore an upper limit on the fraction of bursts that could be associated with nearby Type Ib/c SNe (Kippen et al. 1998). Though model-independent, this limit depends on how coarsely the histogram is binned. It also assumes than an arbitrary distribution of intensities is acceptable for bursts that do *not* come from the homogeneous subpopulation. This is too much freedom, because physically plausible distributions occupy only a subset of all arbitrary intensity distributions.

Here we assume that the bulk of GRBs come from the cosmological distributions discussed in section 3.1. An upper limit on the rate of all GRBs that might come from Type Ib/c SNe (or any nearby homogeneous distribution) is then fixed by determining the maximum rate of bursts that can come from a (differential) distribution proportional to $P^{-5/2}$ before the model becomes inconsistent with the data. We thus fit a model of the form

$$\Delta R(P_1, P_2) = R_H \int_{P_1}^{P_2} dP\ E(P)\ P^{-5/2} + \int_{P_1}^{P_2} dP\ E(P)\ \left\langle \frac{dR}{dP} \right\rangle . \qquad (12)$$

The fractional burst rates corresponding to the 90% and 99% confidence upper limits on the normalization R_H in each model are given in Table 8. The upper limits were determined by finding the value of R_H for which $\Delta\chi^2 = 2.7$ and $\Delta\chi^2 = 6.6$, respectively, when χ^2 is minimized with respect to the other fit parameters (Avni 1976). In all cases, only a modest fraction, 5–10%, of the observed GRBs could come from a homogeneous subpopulation (and thus from nearby SNe). These upper limits are comparable to the model-independent result found in the previous paragraph. They are slightly less constraining because of the fact that our peak flux distribution refers only to the 1.024 s time scale, so it takes no account of the paucity of faint bursts found on the 4.096 and 8.192 s time scales (see section 2.2).

These results were to be expected from the facts that 1) models D1, D2, and D3 with power-law luminosity distributions already gave excellent fits to the data without the presence of the homogeneous ($P^{-5/2}$) term, which is sharply peaked at low peak fluxes, and 2) the fractional uncertainties on the rates in each bin are on the order of 10%. The upper limits discussed here would be further reduced if a given GRB must exhibit certain characteristics (e.g., single-peaked time profile, lack of emission above 300 keV) in order to be considered a candidate S-GRB (Bloom et al. 1998). Norris, Bonnell, & Watanabe (1998) have found that only 0.25–0.5% of BATSE GRBs have temporal and spectral characteristics similar to GRB 980425.

4. Discussion

The GRB peak flux distribution alone (on the 1.024 s time scale) only weakly distinguishes between the non-evolving model $\rho(z)$ = constant (D1) and the evolving models where $\rho(z)$ is proportional to an estimate of the star formation history (D2 and D3). (In this section we restrict our attention to models that include a power-law distribution of intrinsic peak luminosities.) A similar conclusion has been reached previously by Krumholz et al. (1998), who analyze the BATSE catalog data and find that to reliably distinguish the non-evolving and evolving models requires data from more sensitive GRB detectors and/or the measurement of more individual GRB redshifts.

The off-line sample of GRBs constitutes a more sensitive experiment than the one analyzed by Krumholz et al. (1998). Here we argue that models similar (or identical) to D2 and D3, in which the GRB rate has a significant peak in the redshift range $1 < z < 3$, *are modestly preferred over the constant rate density model.* Two independent lines of reasoning serve to denigrate the $\rho(z)$ = constant ("non-evolving") models in favor of the evolving ones.

First, our search on the 1.024 s time scale can reach peak fluxes as low as 0.16 ph cm^{-2} s^{-1} in the 50–300 keV band (50% detection efficiency). But our searches on the 4.096 and 8.192 s time scales are sensitive to peak fluxes (averaged over the matching time scale) that are lower by factors of ~ 2 and $\sim 2\sqrt{2}$, respectively, than the 1.024 s threshold. In fact, most of the bursts we detect have their highest signal-to-noise ratio in the 8.192 s search. Yet surprisingly few bursts are detected *exclusively* on the longer 4.096 s and 8.192 s time scales. This suggests that there are relatively few faint GRBs waiting to be detected by a search that is more sensitive than the one we carried out. In this respect, the evolving models (D2 and D3) appear to be more accurate. They predict that the number of bursts per logarithmic peak flux interval will level off towards lower peak fluxes, and may even start to decline (see Figure 4). The non-evolving model, on the other hand, predicts that the number of bursts observed per logarithmic peak flux interval will continue to increase towards lower peak fluxes.

Since we have not derived peak fluxes on the 4.096 and 8.192 s time scales in order to repeat the analysis of section 3.1, we offer the following quantitative evidence that the paucity of bursts detected on the longer time scales favors the evolving models D2 and D3 over the non-evolving model D1. On the 1.024 s time scale, the measured value of $\langle (C_{min}/C_{max})^{3/2} \rangle = 0.247 \pm 0.006$ is trivially consistent with the values of $\langle (P_{min}/P)^{3/2} \rangle$ found for the best-fit models in section 3.1. But the value of $\langle (C_{min}/C_{max})^{3/2} \rangle = 0.177 \pm 0.006$ found for *all* bursts detected by our search contains information on the paucity of faint bursts on the 4.096 and 8.192 s time scales. We can compare it with the value of $\langle (P_{min}/P)^{3/2} \rangle$ obtained by extrapolating the best-fit models of section 3.1 to the peak flux threshold associated with the 8.192 s search. Taking $0.18/(2\sqrt{2}) =$ 0.06 ph cm^{-2} s^{-1} as the approximate P_{min} for the 8.192 s search, we obtain the following values for $\langle (P_{min}/P)^{3/2} \rangle$: 0.221 in model D1, 0.169 in model D2, and 0.147 in model D3. Thus model D2 produces a value of $\langle (P_{min}/P)^{3/2} \rangle$ that is the most consistent with the value of $\langle (C_{min}/C_{max})^{3/2} \rangle$ found for our full sample, and model D1 produces the most inconsistent value.

Second, the inferred equivalent isotropic peak luminosities (in the 30–2000 keV range) of the 3 bursts for which associated redshifts have been measured can be compared with the effective luminosity distributions of the best-fit models. The best-fit non-evolving model (D1) predicts that 90% of all GRBs should come from the narrow range of intrinsic peak luminosities (0.29–0.66) $10^{51} h_{70}^{-2}$ erg s^{-1} (a factor of $\sim$ 2). The range from which 90% of the *observed* GRBs in this model are drawn is somewhat broader, however: (0.29–1.5) $10^{51} h_{70}^{-2}$ erg s^{-1} (a factor of $\sim$ 5). In contrast, the intrinsic luminosities inferred from the 3 bursts with associated redshift information span a much broader peak luminosity range, (0.6–37) $10^{51} h_{70}^{-2}$ erg s^{-1} (a factor of $\sim$ 62). Bursts with peak luminosities as high as those inferred for GRB 971214 ((37 ± 16) $10^{51} h_{70}^{-2}$ erg s^{-1}) and GRB 980703 ((2.2 ± 0.4) $10^{51} h_{70}^{-2}$ erg s^{-1}) are extremely rare events if the (non-evolving) model D1 is correct. On the other hand, the best-fit (evolving) models D2 and D3 allow a much broader (and uniformly higher) range of luminosities. The best-fit model D2 predicts that 90% of all GRBs are drawn from the intrinsic peak luminosity range (0.50–7.3) $10^{51} h_{70}^{-2}$ erg s^{-1} (a factor of $\sim$ 15) and that 90% of the observed GRBs are drawn from the range (0.53–72) $10^{51} h_{70}^{-2}$ erg s^{-1} (a factor of $\sim$ 130). Likewise, the best-fit model D3 predicts that 90% of all GRBs are drawn from the range (1.5–9.3) $10^{51}h_{70}^{-2}$ erg s^{-1} (a factor of $\sim$ 6) and 90% of the observed GRBs are drawn from the range (1.5–40) $10^{51}h_{70}^{-2}$ erg s^{-1} (a factor of $\sim$ 25). In the context of models D2 and D3, the GRBs 970508, 971214, 980613, and 980703 constitute a much more likely sample of detected bursts than in model D1.

The effective redshift distributions (the rates of observed bursts as a function of redshift) furnish another point of comparison with GRBs 970508, 971214, 980613, 980703. As shown in Figure 5 the model D1 predicts a vanishingly small rate of observed bursts from the redshift $z = 3.418$ measured for GRB 981214 (Kulkarni et al. 1998a). If model D1 were correct, then it would be remarkable that BATSE and *BeppoSAX* detected such a rare burst: only 1×10^{-6} of the rate distribution comes from higher redshifts. On the other hand, the evolving models D2 and D3 predict much higher rates of observed bursts from $z = 3.418$. Even in these models, however, such a high redshift is exceptional: in model D2 only 0.4% of the burst rate distribution lies beyond $z = 3.4$, and in model D3 only 1.8% does. Still, as in the case of the inferred luminosity distributions, the 3 bursts with associated redshifts are a much more likely sample in models D2 and D3, where the GRB rate follows an estimate of the star formation history.

These results certainly do not prove that the GRB rate traces the star formation rate. The peak flux distributions alone fail to exclude the non-evolving rate density model (D1) with high confidence, especially in view of the unknown cosmological parameters which can be varied to improve the fit. Furthermore, until many more redshifts are associated with specific GRBs and/or more sensitive GRB detectors go online, the data will not be able to distinguish qualitatively similar SFR evolution models such as D2 and D3. Any evolution that specifies a significant peak in the burst rate in the redshift range $1 < z < 3$ is likely to be consistent with current data. The reasoning regarding the paucity of faint bursts detected *only* on the 4 s and 8 s time scales should be addressed more quantitatively in the context of the models; but this is difficult owing to our poor understanding of the diverse time profiles of GRBs and of the correlations between time profiles and peak fluxes. Finally, we have considered only 3 very specific "straw-man" models, and it may be that none of them are particularly accurate representations of the true GRB rate density and peak luminosity distributions. For example, a previous episode of star formation at high redshift could contribute a hitherto undetected population of very faint GRBs.

Nevertheless, the results of our search appear to support the conclusions reached by Totani (1997), Wijers et al. (1998), and Krumholz et al. (1998), who showed that if the GRB rate traces the SFR then relatively few faint "classical" GRBs are to be found below the BATSE onboard detection threshold. This information should be useful to the designers and operators of future GRB detectors.

In Figure 6 we plot the cumulative rate distribution of the off-line sample of GRBs along with the best fit models and their extrapolations to lower and higher peak fluxes than are available in the data. The best fit models apparently predict too many bright bursts above the maximum peak flux that was used to fit the differential burst rate (20.0 ph cm^{-2} s^{-1}). This discrepancy is not surprising because the fits did not include data at high peak fluxes. A Kolmogorov-Smirnov (K-S) test (Press et al. 1995) indicates that the discrepancy is not significant if the data and best fit models are compared for *all* peak fluxes above 0.18 ph cm^{-2} s^{-1}. (The probability of getting a larger value of the K-S statistic is 0.4 for model D2.) If the K-S test is restricted to the data above 10.0 ph cm^{-2} s^{-1}, however, the discrepancy is significant (the probability of getting a larger value of the K-S statictic is 6×10^{-4} for model D2). This means that the extrapolations of the best fit models are inaccurate at high peak fluxes.

Future research should explore the peak flux distribution over the widest possible range. For example, the GRB detector onboard *Pioneer Venus Orbiter* (*PVO*) operated for a much longer mission than has BATSE (so far) and it has more completely sampled the rate of very bright bursts. When the peak fluxes of the GRBs detected with *PVO* are calibrated to match the BATSE peak fluxes, it would be of interest to see if the parameters of the best-fit models found in this paper remain consistent with the number counts when the very bright bursts are included. Figure 6 shows that the slopes of the best-fit models approach the $-3/2$ slope reported to be consistent with the brightest *PVO* bursts (Fenimore et al. 1993).

The results of the best-fit models are otherwise generally consistent with previous studies of the BATSE data. In particular we find that while we cannot constrain the full width of the power-law luminosity function in any of the scenarios we considered, the best-fit

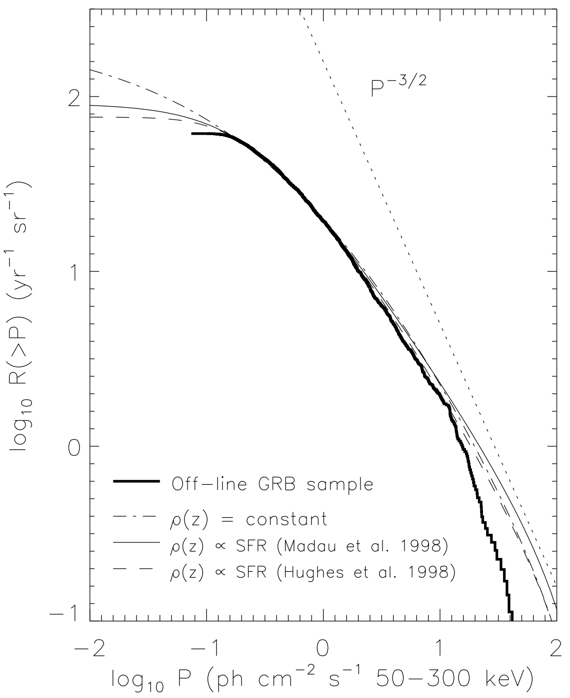

Fig. 6.— Cumulative peak flux distributions for best-fit models. The units of R are bursts yr^{-1} sr^{-1}. The observed peak flux distribution for the off-line sample is shown as the solid histogram. The best-fit model D1 is shown as the dot-dashed line. Model D2 is shown as the solid line. Model D3 is shown as the dashed line. The discrepancy at high peak fluxes is not surprising because the fitting used only data from the interval 0.18–20.0 ph cm^{-2} s^{-1}, but the curves in the figure are intended to reflect true cumulative distributions (with no lower or upper limit on peak flux). The best-fit models appear to predict too many bright bursts, though the discrepancy between the data and the models is not statistically significant unless the comparison is restricted to bright bursts only (data above 10.0 ph cm^{-2} s^{-1}). This suggests that the off-line sample should be combined with data from longer missions, such as *PVO* and/or *Ulysses* to check the behavior of the burst rate at high peak fluxes.

models yield intrinsic peak luminosity functions that contain 90% of all GRBs within a factor of 10–20. This result (or a similar one) has been previously obtained by Ulmer, Wijers, & Fenimore (1995), Woods & Loeb (1995), Hakkila et al. (1996), and Horack et al. (1996). We find that the peak luminosity distribution of the observed bursts, however, is wider: in model D2, 90% of the observed bursts come from a peak luminosity range that spans a factor of ~ 100 or more. A similar result is discussed by Loredo & Wasserman (1998).

The effective redshift distributions that we obtain (see Figure 5) are reasonably consistent with those obtained by Krumholz et al. (1998) and Mao & Mo (1998) using the BATSE catalog data. They are also consistent with limits on the redshifts of GRB sources set by the non-detection of any gravitationally lensed GRBs in the BATSE catalogs (Marani et al. 1998). Holz, Miller, & Quashnock (1998) derive upper limits of $\langle z \rangle = 2.3$ (68% confidence) and $\langle z \rangle = 5.3$ (95% confidence) for the average redshift of GRB sources in the Einstein-de Sitter cosmology. The values of $\langle z \rangle$ we obtain for our best fit models (see Section 3.1) are all well within these limits. The effective redshift distributions are also consistent with the disparity found by Norris et al. (1995) between the duration distributions of bright and dim GRBs, which they interpret as the signature of cosmological time dilation for a GRB source distribution with the dimmest bursts at $z \approx 2$.

On the other hand, our effective redshift distributions are somewhat at odds with the conclusions of Wijers et al. (1998) that the faintest bursts observed with BATSE are at redshifts of $3 < z < 6$. Part of the discrepancy is explained by the fact that rate model used by Wijers et al. (1998) does not correct for the cosmological time dilation of the co-moving burst rate. According to our results with models D1, D2, and D3, no more than 0.002%, 1%, or 5% (respectively) of the bursts observed with our off-line sample are from redshifts larger than $z = 3.0$; and fewer than 8×10^{-7}%, 0.07%, and 0.3%, respectively, are at redshifts greater than $z = 4.0$. So, it is possible that GRBs may be produced at redshifts as high as $z \approx 6$; but even model D3, which allows the highest redshifts, permits only a 7% chance that one or more such bursts have been observed among the 2265 in the off-line sample.

To summarize, our off-line search of archival BATSE data has explored the distribution of GRB intensities at peak fluxes below the onboard detection threshold. We find a paucity of faint bursts detected on the 4.096 and 8.192 s time scales that were not already detected on the 1.024 s time scale. The differential intensity distribution is consistent with models in which the GRB rate traces the global star formation history of the Universe; and it is marginally consistent with the model in which the GRB rate is independent of redshift. We argue that the models in which the GRB rate traces the star formation rate are nevertheless preferred, based on the paucity of faint bursts detected exclusively on the 4.096 s and 8.192 s time scales, and on the comparison of the inferred effective luminosity and redshift distributions with the bursts for which redshifts have been measured. As an application of the off-line GRB intensity distribution, we set a limit of 10% (99% confidence) on the fractional rate of all GRBs that could belong to a homogeneous (in Euclidean space) subpopulation of burst sources (such as Type Ib/c supernovae).

J. M. K. thanks Bob Rutledge for a careful reading of the manuscript, and acknowledges useful discussions with Ed Fenimore, Jon Hakkila, Gabriela Marani, Bob Nemiroff, and Ralph Wijers, as well as support from NASA Graduate Student Researchers Program Fellowship NGT8-52816. W. H. G. L. acknowledges support from NASA under grant NAG5-3804. C. K. acknowledges support from NASA under grants NAG5-32490 and NAG5-4799. J. v. P. acknowledges support from NASA under grants NAG5-2755 and NAG5-3674.

REFERENCES

Avni, Y. 1976, ApJ, 210, 642

Band, D., et al. 1993, ApJ, 413, 281

Bloom, J. S., Kulkarni, S. R., Harrison, F., Prince, T., Phinney, E. S., & Frail, D. A. 1998, ApJ, 506, L105

Cohen, E., & Piran, T. 1995, ApJ, 444, L25

Costa, E., et al. 1997, Nature, 387, 793

Djorgovski, S. G., Kulkarni, S. R., Bloom, J. S., Goodrich, R., Frail, D. A., Piro, L., & Palazzi, E. 1998, ApJ, 508, L17

Djorgovski, S. G., Kulkarni, S. R., Bloom, J. S., Frail, D. A., Chaffee, F., & Goodrich, R. 1998, GCN Circular No. 189

Dunlop, J. S. 1998, in Observational Cosmology with the New Radio Surveys, eds. M. N. Bremer et al. (Netherlands: Kluwer Academic Publishers), 157

Fall, S. M., Charlot, S., & Pei, Y. C. 1996, ApJ, 464, L43

Fenimore, E. E., et al. 1993, Nature, 366, 40

Fenimore, E. E., & Bloom, J. S. 1995, ApJ, 453, 25

Fishman, G. J., et al. 1989, Proceedings of the GRO Science Workshop, 2-39

Fishman, G. J., et al. 1994, ApJS, 92, 229

Frail, D. A., et al. 1997, Nature, 389, 261

Galama, T. J., et al. 1998, Nature, 395, 670

Hakkila, J., et al. 1996, ApJ, 462, 125

Hartmann, D., Blumenthal, G., Chuang, K.-W., Hurley, K., Kargatis, V., Liang, E., & Linder, E. 1992, in Gamma-Ray Bursts Observations, Analyses, and Theories, eds. C. Ho, R. I. Epstein, & E. E. Fenimore (Cambridge: CUP), 45

Higdon, J. C., & Schmidt, M. 1990, ApJ, 355, 13

Holz, D. E., Miller, M. C., & Quashnock, J. M. 1998, astro-ph/9804271

Horack, J. M., Hakkila, J., Emslie, A. G., & Meegan, C. A. 1996, ApJ, 462, 131

Hughes, D. H., et al. 1998, Nature, 394, 241

in't Zand, J. J. M., & Fenimore, E. E. 1994, in Gamma Ray Bursts, AIP Conf Proc. 307, eds. G. J. Fishman, J. J. Brainerd, & K. Hurley (Woodbury, NY: AIP), 692

Iwamoto, K., et al. 1998, Nature, 395, 672

Kippen, R. M., et al. 1998, ApJ, 506, L27

Kommers, J. M., Lewin, W. H. G., van Paradijs, J., Kouveliotou, C., Fishman, G. J., & Briggs, M. S. 1996, in Gamma Ray Bursts, AIP Conf. Proc. 384, eds. C. Kouveliotou, M. S. Briggs, & G. J. Fishman (New York: AIP), 441

Kommers, J. M., Lewin, W. H. G., Kouveliotou, C., van Paradijs, J., Pendleton, G. N., Meegan, C. A., & Fishman, G. J. 1997, ApJ, 491, 704

Kommers, J. M., Lewin, W. H. G., Kouveliotou, C., van Paradijs, J., Pendleton, G. N., Fishman, G. J., & Meegan, C. A. 1998a, in Gamma Ray Bursts, AIP Conf. Proc. 428, eds. C. A. Meegan, R. D. Preece, & T. M. Koshut (New York: AIP), 45

Kommers, J. M., et al. 1999a, ApJ, 511, in press; see also astro-ph/9705171

Kommers, J. M., et al. 1999b, in preparation; http://space.mit.edu/BATSE

Koshut, T. M., Paciesas, W. S., Kouveliotou, C., van Paradijs, J., Pendleton, G. N., Fishman, G. J., & Meegan, C. A. 1996, ApJ, 463, 570

Kouveliotou, C., Meegan, C. A., Fishman, G. J., Bhat, N. P., Briggs, M. S., Koshut, T. M., Paciesas, W. S., & Pendleton, G. N. 1993, ApJ, 413, L101

Krumholz, M., Thorsett, S. E., & Harrison, F. A. 1998, ApJ, 506, L81

Kulkarni, S. R., et al. 1998a, Nature, 393, 35

Kulkarni, S. R., et al. 1998b, Nature, 395, 663

Lilly, S. J., Le Fevre, O., Hammer, F., & Crampton, D. 1996, ApJ, 460, L1

Loredo, T. J., & Wasserman, I. M. 1995, ApJS, 96, 261

Loredo, T. J., & Wasserman, I. M. 1997, astro-ph/9701111

Loredo, T. J., & Wasserman, I. M. 1998, ApJ, 502, 75

Loveday, J., Peterson, B. A., Efstathiou, G., & Maddox, S. J. 1992, ApJ, 390, 338

Madau, P., Della Valle, M., & Panagia, N. 1998, MNRAS, 297, L17

Madau, P., Pozzetti, L., & Dickinson, M. 1998, ApJ, 498, 106

Mallozzi, R. S., Pendleton, G. N., & Paciesas, W. S. 1996, ApJ, 471, 636

Mao, S., & Mo, H. J. 1998, A&A, 339, L1

Marani, G. F., Nemiroff, R. J., Norris, J. P., Hurley, K., & Bonnell, J. T. 1998, in Gamma Ray Bursts, AIP Conf. Proc. 428, eds. C. A. Meegan, R. D. Preece, & T. M. Koshut (New York: AIP), 166

Matz, S. M., Higdon, J. C., Share, G. H., Messina, D. C., & Iadicicco, A. 1992, in Gamma-Ray Bursts Observations, Analyses, and Theories, ed. C. Ho, R. I. Epstein, & E. E. Fenimore (Cambridge: CUP), 175

Meegan, C. A., Fishman, G. J., Wilson, R. B., Paciesas, W. S., Pendleton, G. N., Horack, J. M., Brock, M. N., & Kouveliotou, C. 1992, Nature, 355, 143

Meegan, C. A., et al. 1996, ApJS, 106, 65

Meegan, C. A., et al. 1998, http://www.batse.msfc.nasa.gov/data/grb/catalog

Metzger, M., et al. 1997, Nature, 387, 878

Norris, J. P., Bonnell, J. T., Nemiroff, R. J., Scargle, J. D., Kouveliotou, C., Paciesas, W. S., Meegan, C. A., & Fishman, G. J. 1995, ApJ, 439, 542

Norris, J. P., Bonnell, J. T., & Watanabe, K. 1998, astro-ph/9807322

Ogasaka, Y., Murakami, T., Nishimura, J., Yoshida, A., & Fenimore, E. E. 1991, ApJ, 383, L61

Paciesas, W. S., et al. 1998, ApJS, in press; http://www.batse.msfc.nasa.gov/data/grb/4bcatalog

Press, W., Flannery, B., Teukolsky, S., & Vetterling, W. 1995, Numerical Recipes in C, (Cambridge: CUP)

Rutledge, R. E., Hui, L., & Lewin, W. H. G. 1995, MNRAS, 276, 753

Schaefer, B. E., Cline, T. L., Hurley, K. C., & Laros, J. G. 1997, ApJ, 489, 693

Schechter, P. 1976, ApJ, 203, 297

Schmidt, M., Higdon, J. C., & Hueter, G. 1988, ApJ, 329, L85

Tinney, C., Stathakis, R., Cannon, R., & Galama, T. J. 1998, IAU Circ.No. 6896

Totani, T. 1997, ApJ, 486, L71

Totani, T. 1998, astro-ph/9805263

Ulmer, A., Wijers, R. A. M. J., & Fenimore, E. E. 1995, ApJ, 440, L9

Van Paradijs, J., et al. 1997, Nature, 386, 686

Weinberg, S. 1972, Gravitation and Cosmology: Principles and Applications of the General Theory of Relativity (New York: John Wiley & Sons), 483

Wijers, R. A. M. J., Bloom, J. S., Bagla, J. S., & Natarajan, P. 1998, MNRAS, 294, L13

Woods, E., & Loeb, A. 1995, ApJ, 453, 583

Woods, P., Kippen, R. M., & Connaughton, V. 1998, GCN Circular No. 112

This 2-column preprint was prepared with the AAS LaTeX macros v4.0.

Table 1

Values of $\langle (C_{min}/C_{max})^{3/2} \rangle$ obtained by various GRB detectors.

Detector/Mission	$\langle (C_{min}/C_{max})^{3/2} \rangle$	Reference
PVO	0.46 ± 0.02	Hartmann et al. 1992
Konus/*Venera 11 & 12*	0.45 ± 0.03	Higdon & Schmidt 1990
A4/*HEAO 1*	0.40 ± 0.08	Schmidt, Higdon, & Hueter 1988
GRS/*SMM*	0.40 ± 0.025	Matz et al. 1992
GBD/*Ginga*	0.35 ± 0.035	Ogasaka et al. 1991
BATSE/*CGRO* (3B)	0.33 ± 0.01	Meegan et al. 1996
BATSE/*CGRO* (off-line, 1.024 s search only)	0.247 ± 0.006	(this paper)
BATSE/*CGRO* (all off-line)	0.177 ± 0.006	(this paper)

Table 2

Data for fitting differential peak flux distribution

P_1	P_2	ΔN_{obs}	ΔR (yr^{-1} sr^{-1})
0.180	0.202	87	2.45 ± 0.26
0.202	0.227	83	2.34 ± 0.26
0.227	0.254	99	2.80 ± 0.28
0.254	0.285	111	3.13 ± 0.30
0.285	0.320	92	2.60 ± 0.27
0.320	0.359	96	2.71 ± 0.28
0.359	0.403	95	2.68 ± 0.27
0.403	0.452	114	3.22 ± 0.30
0.452	0.507	93	2.62 ± 0.27
0.507	0.569	79	2.23 ± 0.25
0.569	0.639	82	2.31 ± 0.26
0.639	0.717	91	2.57 ± 0.27
0.717	0.804	73	2.06 ± 0.24
0.804	0.902	83	2.34 ± 0.26
0.902	1.000	52	1.47 ± 0.20
1.000	1.259	117	3.30 ± 0.31
1.259	1.584	111	3.13 ± 0.30
1.584	1.995	104	2.93 ± 0.29
1.995	2.511	72	2.03 ± 0.24
2.511	3.162	59	1.66 ± 0.22
3.162	3.981	48	1.35 ± 0.20
3.981	5.011	40	1.13 ± 0.18
5.011	6.309	27	0.76 ± 0.15
6.309	7.943	26	0.73 ± 0.14
7.943	20.00	64	1.80 ± 0.23

Table 3

Redshifts and implied equivalent isotropic peak luminosities

GRB	Peak Flux (50–300 keV)	z	Implied L ($10^{51} h_{70}^{-2}$ erg s^{-1} in 30–2000 keV)
970508	0.97 ± 0.05[a]	0.835[c]	0.6 ± 0.1
971214	1.95 ± 0.05[a]	3.418[d]	37 ± 16
980613	0.63 ± 0.05[b]	1.096[e]	0.8 ± 0.2
980703	2.39 ± 0.06[a]	0.966[f]	2.2 ± 0.4

[a]Meegan et al. (1998)

[b]Woods, Kippen, & Connaughton (1999)

[c]Metzger et al. (1997)

[d]Kulkarni et al. (1998a)

[e]Djorgovski et al. (1999)

[f]Djorgovski et al. (1998)

Table 4

Best fit parameters for monoluminous cosmological models

$\rho(z)$	R_0 (h_{70}^3 Gpc^{-3} yr^{-1} sr^{-1})	L_0 (10^{51} h_{70}^{-2} erg s^{-1})	χ^2 (23 d.o.f)
D1 (constant)	$9.45^{+0.39}_{-0.78}$	$0.40^{+0.06}_{-0.02}$	32.3
D2 (SFR)	2.0 ± 0.1	1.5 ± 0.1	64.1
D3 (AGN)	1.9 ± 0.1	$3.1^{+0.4}_{-0.2}$	27.8

Table 5

Best fit parameters for cosmological models with a power-law luminosity function

$\rho(z)$	R_0 (h_{70}^3 Gpc^{-3} yr^{-1} sr^{-1})	L_{min} (10^{51} h_{70}^{-2} erg s^{-1})	β	χ^2 (22 d.o.f)
D1 (constant)	8.8 ± 1.3	$0.29^{+0.08}_{-0.06}$	$4.6_{-1.4}$[a]	32.9
D2 (SFR)	2.2 ± 0.3	$0.48^{+0.20}_{-0.10}$	$2.1^{+0.3}_{-0.2}$	17.9
D3 (AGN)	2.1 ± 0.2	$1.44^{+0.53}_{-0.40}$	$2.6^{+1.0}_{-0.4}$	17.4

[a]This parameter is not constrained above the the best fit value when the other parameters are free to vary.

Table 6

Co-moving $z = 0$ burst rate for monoluminous cosmological models

$\rho(z)$	ρ_0 (h_{70}^3 Gpc^{-3} yr^{-1})	GEM[a] (Myr^{-1})
D1 (constant)	$11.9^{+0.5}_{-1.0}$	~ 2
D2 (SFR)	0.78 ± 0.04	~ 0.2
D3 (AGN)	0.46 ± 0.02	~ 0.1

[a]Galactic Events per Million years.

Table 7

Co-moving $z = 0$ burst rate for cosmological models with a power-law luminosity function

$\rho(z)$	ρ_0 (h_{70}^3 Gpc^{-3} yr^{-1})	GEM[a] (Myr^{-1})
D1 (constant)	11.1 ± 1.6	~ 2
D2 (SFR)	0.87 ± 0.12	~ 0.2
D3 (AGN)	0.51 ± 0.05	~ 0.1

[a]Galactic Events per Million years.

Table 8

Upper limits on fractional GRB rate due to a possible homogeneous (in Euclidean space) sub-population of GRBs

$\rho(z)$	90%	99%
D1 (constant)	5.1%	6.2%
D2 (SFR)	6.9%	10.0%
D3 (AGN)	7.7%	11.2%